

A NEW APPROACH TO THE MODELING OF THE TRANSFER FUNCTION OF THE POWER LINE CHANNEL

T.C. Banwell, S. Galli

{bct, sgalli}@research.telcordia.com

Telcordia Technologies, Inc., 445 South Street, Morristown, NJ 07960, USA

Abstract – The “indoor” access network is characterized by several branches and impedance mismatches that cause many reflections. In the present paper, a new way of modeling the transfer function of a power line is proposed. The proposed model starts by considering the power line channel as a uniform transmission line. This allows the power line channel to be described as a cascade of simple two-port networks, each of which may be easily described with its transmission matrix. This approach allows us to model in the frequency domain any power line channel, regardless of its topology, by considering as special two-port networks any series or shunt impedances (i.e., branches) present along the line. This approach also implies the validity of the TEM approximation. It is possible to prove that this assumption is valid assuming correct mode excitation, which differs from conventional twisted pair. In so doing, the usual problems encountered in the time-domain characterization of the power line channel as a multipath channel can be avoided. Interestingly, the transmission matrices approach allows us also to show the existence of a particular symmetry of the power line channel that was not previously revealed [5].

Keywords: *power line channel models, frequency transfer functions, transmission matrices.*

1. Introduction

Considerable effort has been recently devoted to the determination of accurate channel models for the power line (PL) environment, both for the indoor and outdoor cases. However, the characterization of the transfer function is a non-trivial task to achieve since PL characteristics may change due to the particular topology of a given link.

There are several approaches that have been followed for the characterization of the power line channel (PLC) [1]. In particular, an interesting approach is to describe the PLC as if it were affected by multipath effects only. In fact, as is well known, the multipath nature of the PLC arises from the presence of several branches and impedance mismatches that cause many reflections. Although this approach has proven to yield a good match between measurements and theoretical model [2], there are at least two major disadvantages in using this method. Firstly, there is a high computational cost in estimating the delay, the amplitude and the phase associated with each path. Secondly, since it is a time-domain approach, it is also necessary to take into consideration the very high number of paths associated with all the possible reflections from the unmatched terminations along the line.

In the present paper, a new approach to the characterization of the PLC is proposed. First the equivalent circuits of the differential mode and the pair mode propagating along the cable are derived. Then, the derived circuit model is represented in terms of cascaded two-port networks (2PNs). Once the equivalent 2PN representation is obtained, it is straightforward to represent the power line link by means of transmission matrices, or ABCD matrices. The possibility of representing a power line link as a cascaded 2PN allows the definition of a model in the frequency domain that can fully take into consideration the particular topology of the link. This is very useful because the description of multiple echoes travelling along a line is better achieved in the frequency domain than in the time domain. In fact, a frequency-domain model contains the composite of all the signals reflected by the discontinuities, whereas a time-domain reflection measurement shows only the effect of each discontinuity. Following this approach, the aforementioned computational cost of describing independently each path in the time-domain disappears. Finally, the possibility of describing the power line cable by means of ABCD matrices allows us to unveil an interesting symmetry property of the power line that has never been pointed out in the previous literature [5].

2. Theoretical and Experimental Validation of the ABCD Modeling

The two predominant types of cable used for indoor power distribution, 12/2 and 14/2, consist of “hot” (black), “return” (white) and ground wires. Let the wire voltages be V_{BLK} , V_{WHT} and V_{GND} , respectively. These three conductor cables support three propagating modes (TEM approximation) which can be described by

$$I^+ + I^- \equiv \begin{pmatrix} I_{dif} \\ I_{pr} \\ I_{cm} \end{pmatrix} = \begin{bmatrix} 0.5 & -0.5 & 0 \\ 1-\theta & 1-\theta & 1-\theta \\ 1 & 1 & 1 \end{bmatrix} \begin{pmatrix} I_{BLK} \\ I_{WHT} \\ I_{GND} \end{pmatrix} \equiv BI_c,$$

$$V^+ + V^- \equiv \begin{pmatrix} V_{dif} \\ V_{pr} \\ V_{cm} \end{pmatrix} = \begin{bmatrix} 0.5 & -1 & 0 \\ 0.5 & 0.5 & -1 \\ 0.5\theta & 0.5\theta & 1-\theta \end{bmatrix} \begin{pmatrix} V_{BLK} \\ V_{WHT} \\ V_{GND} \end{pmatrix} \equiv AV_c.$$

The factor θ describes the shielding produced by the ground: complete shielding gives $\theta = 0$ (BX type), while $\theta \approx 0.5$ for unshielded cables (NM type). It is useful to note that $\mathbf{B}^{-1} = \mathbf{A}^T$ and $\mathbf{A}^{-1} = \mathbf{B}^T$. Figure 1 shows the corresponding equivalent circuit describing the deconvolution of propagating modes. The differential mode I_{dif} represents current confined to white and black wires and is generally the desired signal. The pair mode I_{pr} represents current flowing between the ground wire and the active pair “tied together”. The two modes I_{dif} and I_{pr} are well confined to the cable and consequently exhibit low attenuation. The characteristic impedances associated with these modes measured using TDR are presented in Figure 2. The net common mode current I_{cm} is highly dependent on cable installation. The characteristic impedance for this lossy mode is variable and not readily characterized: $|Z_{cm}| \approx 150\text{-}250\Omega$.

The propagating voltages and currents are related by $\mathbf{V}_1^+ = \mathbf{Z}_o \mathbf{I}_1^+$ and $\mathbf{V}_1^- = \mathbf{Z}_o \mathbf{I}_1^-$, where \mathbf{Z}_o is the diagonal matrix of characteristic impedances. Discontinuities in cables due to interconnections and termination mismatches induce coupling between modes. Consider a semi-infinite cable excited by a purely differential incident wave $\mathbf{I}_1^+ = (I_{dif}^+, 0, 0)$ and whose termination is represented by an impedance matrix \mathbf{Z}_{term} . The boundary condition in this case is $\mathbf{V}_{c1} = \mathbf{Z}_{term} \mathbf{I}_{c1}$. Expressed in terms of the propagating modes, the voltages and currents satisfy $\mathbf{I}_1^+ - \mathbf{I}_1^- = \mathbf{B} \mathbf{I}_{c1}$ and $\mathbf{V}_1^+ - \mathbf{V}_1^- = \mathbf{A} \mathbf{Z}_{term} \mathbf{I}_{c1}$ at the termination. Combining these relationships yields:

$$(\mathbf{Z}_o + \mathbf{A} \mathbf{Z}_{term} \mathbf{A}^T) \mathbf{I}_1^- = (\mathbf{A} \mathbf{Z}_{term} \mathbf{A}^T - \mathbf{Z}_o) \mathbf{I}_1^+,$$

which can be recognized as a generalization of the usual reflection coefficient. The corresponding equation describing the effect of a series impedance \mathbf{Z}_{se} is $(\mathbf{Z}_o + \frac{1}{2} \mathbf{A} \mathbf{Z}_{se} \mathbf{A}^T) \mathbf{I}_1^- = \frac{1}{2} \mathbf{A} \mathbf{Z}_{se} \mathbf{A}^T \mathbf{I}_1^+$, while the effects of a shunt conductance \mathbf{Y}_{sh} are described by $(\mathbf{1} + \frac{1}{2} \mathbf{B} \mathbf{Y}_{sh} \mathbf{B}^T \mathbf{Z}_o) \mathbf{I}_2^+ = \frac{1}{2} \mathbf{A} \mathbf{Z}_{se} \mathbf{A}^T \mathbf{I}_1^+$ and $\mathbf{I}_1^- = \mathbf{I}_2^+ - \mathbf{I}_1^+$. These relationships can be applied iteratively to partition complex cable topologies. In particular, two systems of ABCD matrices can be derived for the differential and pair mode response. Strong coupling between these two modes occurs at a few points in PLN, most notably at the point of ground bonding at the breaker box, the mains feed, and lighting circuits interrupted by switches. Since lighting and outlet circuits are usually fed from separate breakers, the effects of lighting circuits are often masked by the effects of bonding.

A wiring model representing two rooms with four outlets is shown in Figure 3(A). NM-B 14/2 cable was chosen for easier handling. US National Electric Code (NEC) grounding practices were followed. Figure 3(B) shows the connections within the breaker box, including bonding of the return line to ground through R_s . Transmission experiments were conducted between nodes (X) and (Y) in this model. TDR measurements were performed from (X) or (W) using the circuit shown in Figure 4, which produces unipolar $\pm 5V_{OC}$ excitation through a selectable reference impedance (100 Ω or 135 Ω). Differential mode signals are sensed by a difference amplifier having 0.2V/V gain. In some cases, R2 was a 50 Ω scope input that measured pair-mode signals. Swept frequency transmission measurements were performed between (X) and (Y) from 0.3-30MHz. 1: $\sqrt{2}$ transformers were used with resistor matching networks to interface the 50 Ω network analyzer ports to the test points. Experiments were conducted with various values chosen for R_s , R_1 , R_2 , R_3 and R_Y . Specific reflections and resonant modes could be isolated by selectively disconnecting the bonding shunt, 15ft, 25ft and 60ft branches, which results in 12 distinct topology variations.

The equivalent circuit for the model is shown in Figure 5 for excitation at (X). The upper section describes differential mode propagation while the lower section (the “companion” model) describes pair-mode excitation. Due to the high common mode impedance Z_{cm} and long mains length, the predominant coupling between differential and pair modes occurs through R_s alone. Shunt R_s creates a differential mode reflection $\rho_{dif} = -[R_s(n-1) + Z_{dif}/4 + Z_{pr}(n-1)/(n+1)] / [R_s(n+1) + Z_{dif}/4 + Z_{pr}]$, where n is the number of bonded cables. In our case, $\rho_{dif} \approx -0.37$ for $n=2$ type 14/2 cables and $R_s = 0$. The corresponding pair mode excitation is approximately $2Z_{pr} / (Z_{dif} + 4Z_{pr}) \approx 0.32$.

Figure 6 shows the differential TDR and pair-mode excitation seen at W induced by ground bonding alone (mains feed disconnected) using a 135Ω reference impedance. The upper trace in Figure 6 is the differential mode response. The first downward peak is the incident excitation. There is an inverted reflection at 72nsec with $\rho_{\text{dif}} = -0.28$. The lower trace in Figure 6 shows the induced pair mode response having a transmission coefficient of 0.24. The measured amplitudes only differ with theory by 7%, allowing for -0.9dB/25ft cable attenuation measured with open and shorted 25ft sections of cable.

3. An Example of the Computation of the Transfer Function of a Power Line Link by Means of Cascaded Two-Port Networks

The equivalent cascaded 2PN representation of the circuit in Figure 5 will now be derived. Without loss of generality, we will consider the particular case of $R_1=0$, $R_S=2\ \Omega$, and $R_2=R_3=\infty$. Since the companion models in Figure 5 allow us to consider the three-conductor power line link as if it were constituted by only two conductors, we can represent the topology of Figure 3A as the one shown in Figure 7. As described in Section 2.3 of [5], bridged taps can be viewed as a three-port network, where one of the ports appears as a load impedance to the line between the two sections on each side of the bridged tap. Therefore a bridged tap can be viewed as a shunt impedance across the “hot” and “return” cables, with the impedance equal to the input impedance seen looking into the bridged tap. The transformer that “ties” together the differential model and its companion model describing the pair-mode propagation is inserted onto the “hot” and “return” cables as if it were a bridged tap. This means that it appears as a shunt impedance across the “hot” and “return” and the impedance is equal to the input impedance seen looking into the transformer. We can now represent the power line link in Figure 7 as cascaded 2PNs as shown in Figure 8A. With respect to Figure 8A, we have the following definitions:

- T_L : T matrix of a 14/2 cable L feet long;
- $T_L^{(BTU)}$: T matrix of a 14/2 cable L feet long put as an *unterminated* bridged tap onto the main cable (hot – return);
- $T_{60}^{(BTS)}$: T matrix of a 6/2 cable 60 feet long put as an *shorted* bridged tap onto the main cable (hot – return);
- $T_{\text{brk}}^{(BT)}$: T matrix representing the breaker (return -ground shorted).

The superscripts (BT), (BTS), and (BTS) mean that the T matrix has the structure of a shunt impedance across hot and return. The structure of this particular T matrix can be found in eq.(10), Section 2.3 of [5]. Except for the matrix $T_{\text{brk}}^{(BT)}$, the computation of the matrices defined above is trivial and is here skipped. As far as the computation of matrix $T_{\text{brk}}^{(BT)}$ is concerned, it is useful to represent the companion model in Figure 5 as cascaded 2PNs. This is shown in Figure 8B. The input impedance of the 2PN in Figure 8B is Z_B . Therefore, matrix $T_{\text{brk}}^{(BT)}$ has the following structure:

$$T_{\text{brk}}^{(BT)} = \begin{vmatrix} 1 & 0 \\ 1/Z_B & 1 \end{vmatrix}$$

The overall ABCD matrix from (X) to (Y) can be found exploiting the so called *chain-rule* (see section 2.2 in [5]) that states that the overall ABCD matrix of the end-to-end circuit is obtained by multiplying the ABCD matrices of the single portions of the network. Finally, we may represent the power line link in Figure 3A, as the simple circuit shown in Figure 9 where T_{overall} is given by:

$$T_{\text{overall}} = T_{25} \cdot T_{15}^{(BTU)} \cdot T_{25} \cdot T_{60}^{(BTS)} \cdot T_{\text{brk}} \cdot T_{25} \cdot T_{25}^{(BTU)}$$

Once the overall ABCD matrix of the end-to-end circuit is obtained, the transfer function from is given by (see eq. (4) in [5]):

$$H_{XY}(f) = \frac{V_Y}{V_X} = \frac{Z_Y}{AZ_Y + B + CZ_X Z_Y + DZ_X}$$

On the basis of the results contained in [5], the relationship $H_{XY}(f)=H_{YX}(f)$ also holds.

4. Experimental Results

Figure 3 in [5] shows the measured transmission on the link in Figure 3A from (X) to (Y) and (Y) to (X) with $R_1=0$, $R_S=2\ \Omega$ and $R_2=R_3=\infty$. The response is nearly identical in both directions with matched sending and receiving impedance of 140Ω. That figure can be compared with Figure 10 here that shows the transfer function obtained using the equivalent cascaded 2PN representation derived in Section 3. There are some differences in the gains and in the shape of Figure 10 here and Figure 3 in [5]. These differences are essentially due to the fact that our software simulator could only compute ABCD matrices of telephone cable-like gauges (i.e., American

Wire Gauge 19, 22, 24, 26). Therefore, the ABCD calculation in our computer analysis was made using 19 AWG and modifying its characteristic impedance and propagation constant appropriately, but not perfectly. Nevertheless, the similarity of the two figures is striking.

5. References

- [1] H. Philipps, "Modeling of Power Line Communications Channels", *IEEE International Symposium on Power Line Communications and its Applications*, ISPLC'99, Lancaster, UK, April 1999.
- [2] J. Barnes, "A Physical Multi-Path Model for Power Distribution Network Propagation *IEEE International Symposium on Power Line Communications and its Applications*, ISPLC'98, Tokyo, March 1998.
- [3] H. Philipps, "Development of a Statistical Model for Power Line Communications Channels", *IEEE International Symposium on Power Line Communications and its Applications*, ISPLC'00, Limerick, Ireland, April 2000.
- [4] *Transmission Systems for Communications*, Bell Laboratories, Fifth edition, 1982.
- [5] T.C. Banwell, S. Galli, "On the Symmetry of the Power Line Channel", *IEEE International Symposium on Power Line Communications and its Applications*, ISPLC'01, Malmo, Sweden, April 4-6, 2001.

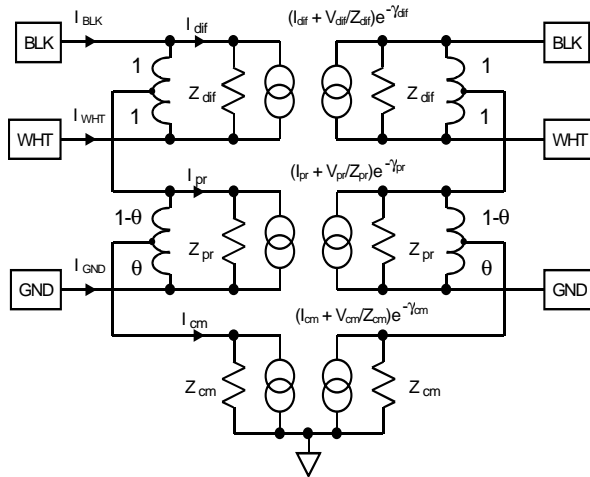


Fig. 1

TYPE	Z _{diff}	Z _{pr}
14/2	140	58
12/2	135	54
10/2	120	48
BX		
12/2	73	52

Fig. 2

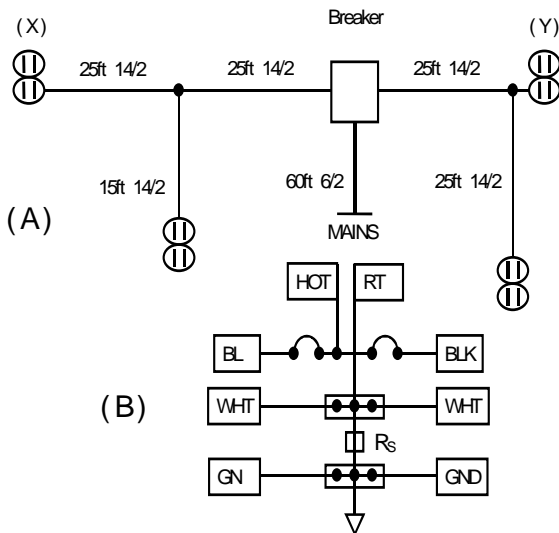


Fig. 3

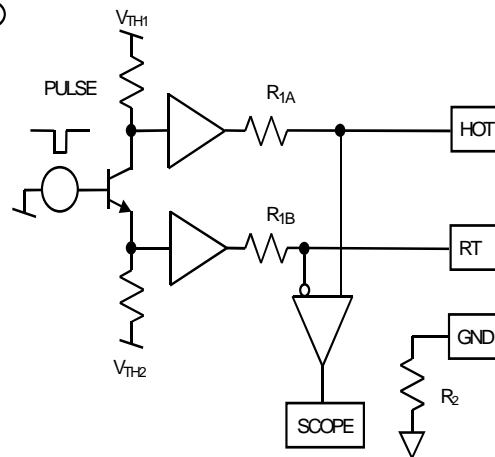


Fig. 4

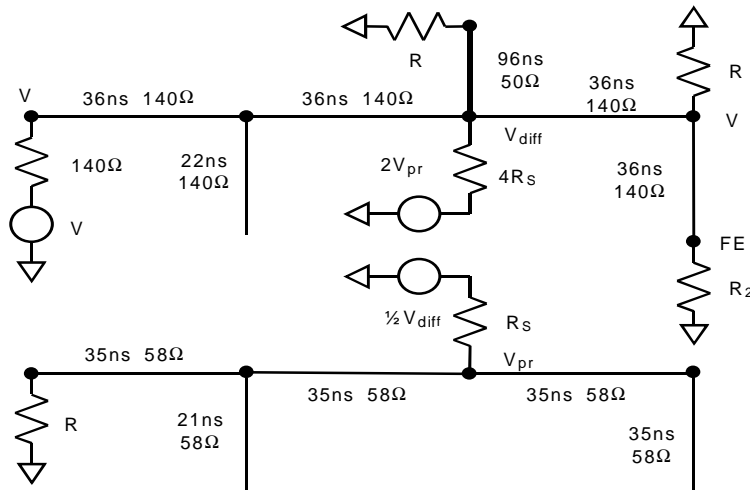


Fig. 5

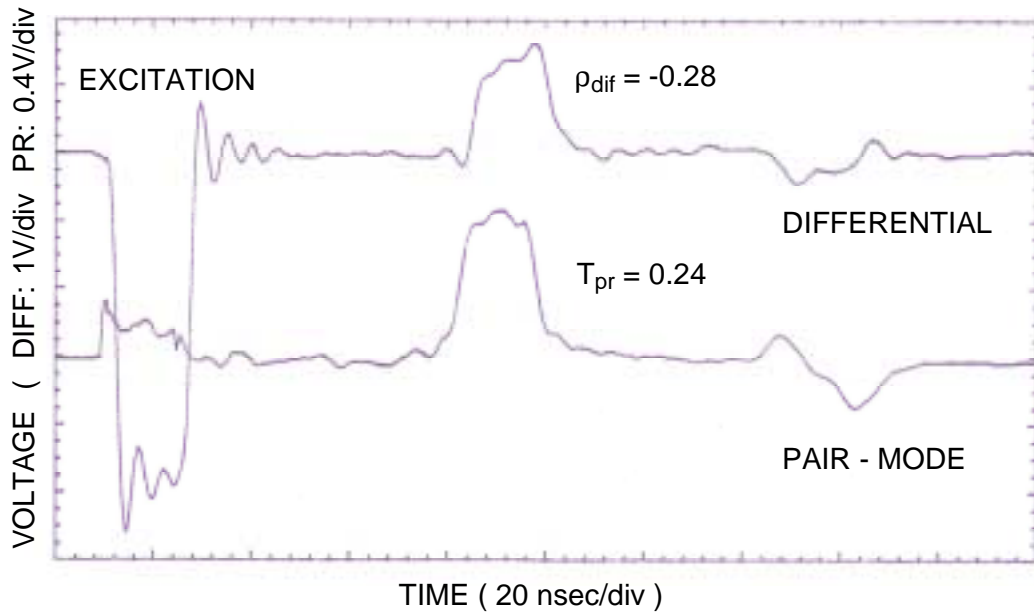


Fig. 6

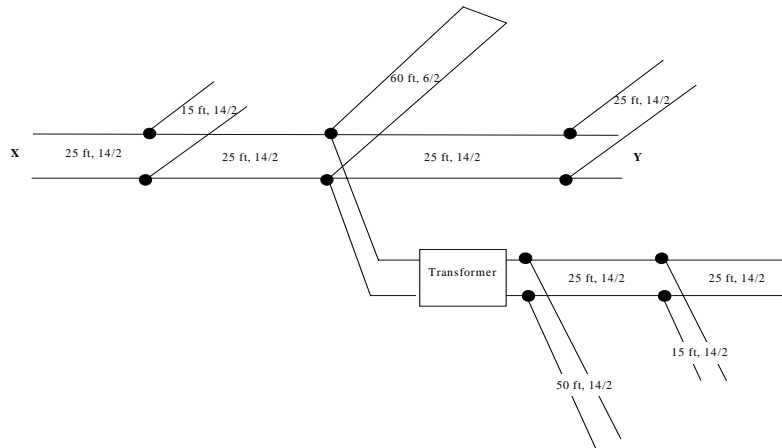


Fig. 7

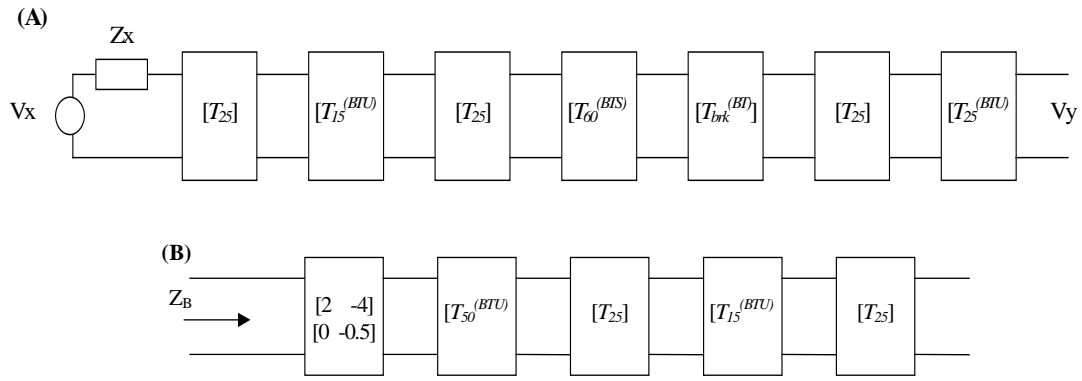


Fig. 8

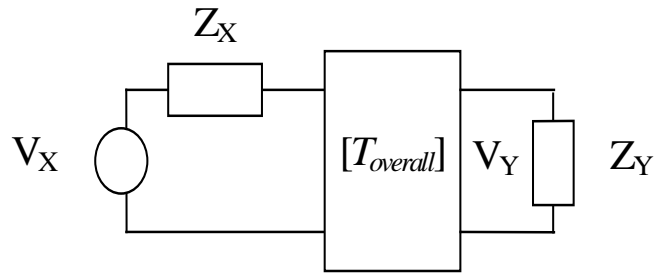


Fig. 9

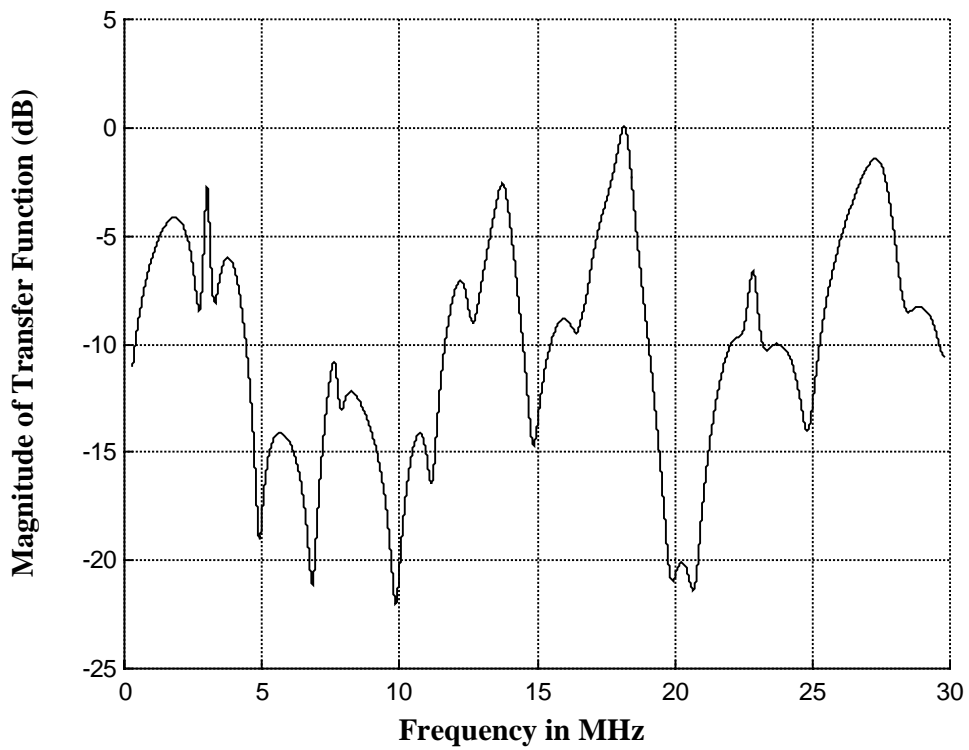


Fig. 10